Journal of Alloys and Compounds 509 (2011) 2535–2539

Contents lists available at ScienceDirect

Journal of Alloys and Compounds

journal homepage: www.elsevier.com/locate/jallcom

Nanometric $La_{0.9}Sr_{0.1}Ga_{0.8}Mg_{0.2}O_{3-x}$ ceramic prepared by low-pressure reactive spark-plasma-sintering

H. Borodianska[a,b], P. Badica[a,c], T. Uchikoshi[a], Y. Sakka[a], O. Vasylkiv[a,*]

[a] National Institute for Materials Science, 1-2-1 Sengen, Tsukuba, Ibaraki, 305-0047, Japan
[b] Institute for Problems in Materials Science of NASU, Krzhizhanovsky, Kiev, 03680, Ukraine
[c] National Institute of Materials Physics, Atomistilor 105bis, Magurele, 077125, Romania

ARTICLE INFO

Article history:
Received 6 August 2010
Received in revised form 6 November 2010
Accepted 11 November 2010
Available online 19 November 2010

Keywords:
LSGM
Spark-plasma-sintering
Electrolyte
SOFC
Nano ceramic

ABSTRACT

It is proposed a processing route to obtain dense (≥90%) nanometric $La_{0.9}Sr_{0.1}Ga_{0.8}Mg_{0.2}O_{3-x}$ (LSGM) electrolyte ceramic by reacting under spark-plasma-sintering (SPS) conditions a relatively poor mixture of intermediate powdered La/Sr- and Ga/Mg-based products synthesized separately by precipitation and hydrothermal methods, respectively. Samples with particle size of 9–20, 37–93, and 120–240 nm were measured from the electrical conductivity viewpoint. A fast transport path along grain boundaries was not observed and, a higher nano particle size improves total conductivity in our samples. Results suggest that it is necessary to make a clear distinction between particle size from microscopy observation and crystallite size from structural (e.g. XRD) measurements when looking at the general conductivity – grain size dependence. This dependence is complex and the use of an unconventional, far from equilibrium technique such as SPS might influence it. Currently, a good understanding is missing, but pending on materials, technology specifics and the complex relationship between them, some of the usually promoted ideas from literature such as the necessity of high mixing levels in the precursor powders, of high pressure application during sintering, of low particle size (nano) in the sintered ceramic for a higher conductivity, of high purity phase and so on require careful consideration.

1. Introduction

Bulk solid-state electrolytes are of much interest for applications in solid-state fuel cells (SOFC). Several ionic oxides are currently considered as strong candidates for electrolytes, but also for oxygen sensors. Among them $La_{1-a}Sr_aGa_{1-b}Mg_bO_{3-x}$ ($x = a/2 + b/2$, LSGM), which is derived from the parent material $LaGaO_3$ [1] shows high ionic conductivity at relatively lower temperatures vs. other candidates, negligible electronic conductivity in a broad range of temperatures and oxygen partial pressures, and good stability over long operating time. However, this material is also well known to have the following problems:

(a) Control of composition and of phases is difficult in LSGM ceramic. Very often the resulting LSGM ceramic contains impurity phases. To remove impurity phases, long reaction times (typically 10–40 h) and high temperatures (>1400 °C) are required [2,3]. Especially this seems to be the case when applying conventional sintering on calcinated (oxide) reacted precursors. To overcome the indicated difficulty, several works proposed improvement of homogeneity and the decrease of the particle size in the reacted precursor (e.g. [4]). On the other hand, it is noteworthy that there are articles [5,6] suggesting that due to the percolative nature of the transport properties in the polycrystalline bulks a certain amount of the impurity phases in the final sintered ceramic, pending also on morphology, might not be critical.

(b) A ceramic electrolyte for SOFC should have high density. But, LSGM is a difficult to consolidate material by conventional sintering. High temperatures are necessary (as already indicated in the previous paragraph) with the main disadvantage being fast and excessive coarsening of grains in the ceramic. Proposed solutions were microwave-assisted sintering of certain types of powders [5,7,8], and pressure assisted methods such as hot isostatic pressing [9] or, recently, high-pressure spark-plasma-sintering [10–12]. From all the sintering methods only the last one allowed formation of dense LSGM ceramic with particle size below 100 nm [10,12].

(c) Reports indicate on evaporation of Sr, Ga and Mg from LSGM at high temperatures [13] and of Ga and Mg at intermediate temperatures and in environments specific for SOFC working conditions [14]. Other general electrical and thermo-mechanical requirements for an electrolyte are presented in Ref. [15].

* Corresponding author. Tel.: +81 0 29 859 2673; fax: +81 0 29 859 2401.
E-mail address: oleg.vasylkiv@nims.go.jp (O. Vasylkiv).

0925-8388/$ – see front matter © 2010 Elsevier B.V. All rights reserved.
doi:10.1016/j.jallcom.2010.11.079

The interest for nano sized material for ionic electrolyte applications is motivated by the possibility to control and virtually improve the transport properties taking advantage of the nano effects at interfaces and/or near interface regions. For zirconia- and ceria-based solid electrolytes nano effects are reviewed in Ref. [16]. Investigation of nano effects is of high interest also for LSGM electrolyte. For this purpose nano sized material is required, but at present there are a limited number of reports [10,12].

In this article we propose a route to obtain dense nano sized LSGM ceramic with particle size down to 9–20 nm. The key idea is to realize in one step the fast reaction between the La/Sr- and Ga/Mg-based intermediate powdered products (unreacted) obtained by precipitation and hydrothermal synthesis, respectively, and sintering of the newly formed $La_{0.9}Sr_{0.1}Ga_{0.8}Mg_{0.2}O_{3-x}$ phase. To implement this idea in our experiments we used low-pressure reactive spark-plasma-sintering. Conductivity of the as-prepared $La_{0.9}Sr_{0.1}Ga_{0.8}Mg_{0.2}O_{3-x}$ ceramic with different nano grain sizes is presented and compared with literature results.

2. Experimental

Raw materials $LaCl_3{\cdot}7H_2O$, $SrCl_2{\cdot}6H_2O$, $GaCl_3$, $MgCl_2{\cdot}6H_2O$ (99.9% purity from Wako Pure Chemicals Co., Japan) were weighted and separately dissolved in distilled and deionized water at a concentration of 0.1 M.

La-based and Sr-based solutions were mixed and hexamethylenetetramine ($C_6H_{12}N_4$) (Wako Pure Chemicals, Co., Japan) was added as a precipitation agent to produce a La/Sr-based intermediate solid product.

For the synthesis of Ga/Mg-based product we tried two approaches:

In the first one, Ga and Mg-based solutions were mixed at low temperature (2 °C). This mixture was sprayed into a 0.5 M aqueous solution of hexamethylenetetramine preliminary cooled at 2 °C and continuously stirred at a high speed of 750 rpm. Cooling and stirring conditions were necessary to prevent strong agglomeration due to the very fast forming of the Ga/Mg-based precipitates. Despite of extreme conditions use, the product was agglomerated into relatively large particles. Attempts to use nitrates as raw materials did not show improvements, and on contrary uniformity of the aggregates size was lower and larger sizes were observed. In these circumstances we decided to use hydrothermal synthesis.

Within this second approach, a stock aqueous solution of concentration 0.1 M of (0.8 Ga^{3+} + 0.2 Mg^{2+}) and 0.5 M urea (NH_2CONH_2, 99% purity, produced by High Purity Chemicals Co., Saitama, Japan) was magnetically stirred at room temperature for 24 h. The 200 ml of mixed urea-contained-sol in which the initial pH was ~ 2, after homogenization was hydrothermally treated in a 250 ml teflon vessel at 110 °C for 50 h. The urea decomposed into NH_3 and CO_2 through reaction with H_2O and the sol's pH changed to ~ 8.5. The precipitate formed was hydrous (0.8 Ga^{3+}/0.2 Mg^{2+}) intermediate complex product, which crystallized under hydrothermal conditions.

As-prepared La/Sr- and Ga/Mg-based intermediate solid products were mixed in the colloidal suspension state (using ultrasound bath) and dried at 75 °C for 50 h under stirring with gradually decreasing rate (from 750 to 100 rpm). Resulting powder mixture was loaded (0.5 g) into a graphite die (10 mm in diameter) with punches and submitted to reactive spark plasma processing. We used Sumitomo Coal Mining SPS system, 'Dr. Sinter', model 1050 (Japan). A low pressure of 25 MPa and a vacuum of 4.5 Pa were initially applied before heating the powder with 500 °C/min under a pressure of maximum 100 MPa, and up to 900 °C. After 2 min holding at this temperature for equipment stabilization heating continued with different heating rates up to the final temperature of 1200 °C or more by applying a starting current of 1000 A. The corresponding voltage was between 3.0 and 4.5 V. A pulsed current pattern of 12-on/2-off pulses was used. After holding the samples at the final desired temperature for 5 min and under the maximum pressure, the applied electrical current was stopped, and the sample was gradually cooled down to 600 °C at a cooling rate of 20 °C/min and subsequently by furnace cooling to room temperature. Pressure was released gradually below 600 °C.

X-ray diffraction measurements were performed at room temperature (Rigaku RINT 2000, Japan, Cu Kα-radiation). Microstructural observations and local compositional analysis measurements were taken with JEOL JEM-2100F and JEOL JSM 7001F (Japan) electronic microscopes equipped with energy dispersive systems. The density of the samples was measured using Archimedes method. For conductivity characterization by complex impedance spectroscopy, Pt-paste electrodes were applied and dried in the air at 900 °C for 0.5 h. Measurements were done in the air and at various temperatures. An impedance analyzer (Hewlett Packard HP 4194A) working in the range of 100 Hz–15 MHz was used.

3. Results and discussion

Morphology of the intermediate La/Sr- and Ga/Mg-based products can be visualized in Fig. 1. Ga/Mg-based product has a rod morphology (Fig. 1(a)). Length is between 0.5 and 3 μm, and diameter is between 50 and 350 nm. Particles of La/Sr-based product are of sphere-like with size of about 20–50 nm agglomerated into aggregates of 300–750 nm of sphere or ellipsoidal shape. EDS confirmed the desired ratio La/Sr and Ga/Mg for each type of intermediate products. Although the products are in the nanosize region, their very different shape makes mixing very difficult. Poor degree of mixing is expected according to literature data [4] to have a possibly negative influence on the uniformity of LSGM phase formation and purity in the final ceramic. Many authors noted that single LSGM ceramic is difficult to be obtained and suggested that smaller particle size may improve the mixing degree. It is important to note that other factors such as agglomeration and nanoparticle morphology, or type of the powders should to be also considered, and, very often, reported data on LSGM synthesis does not present these

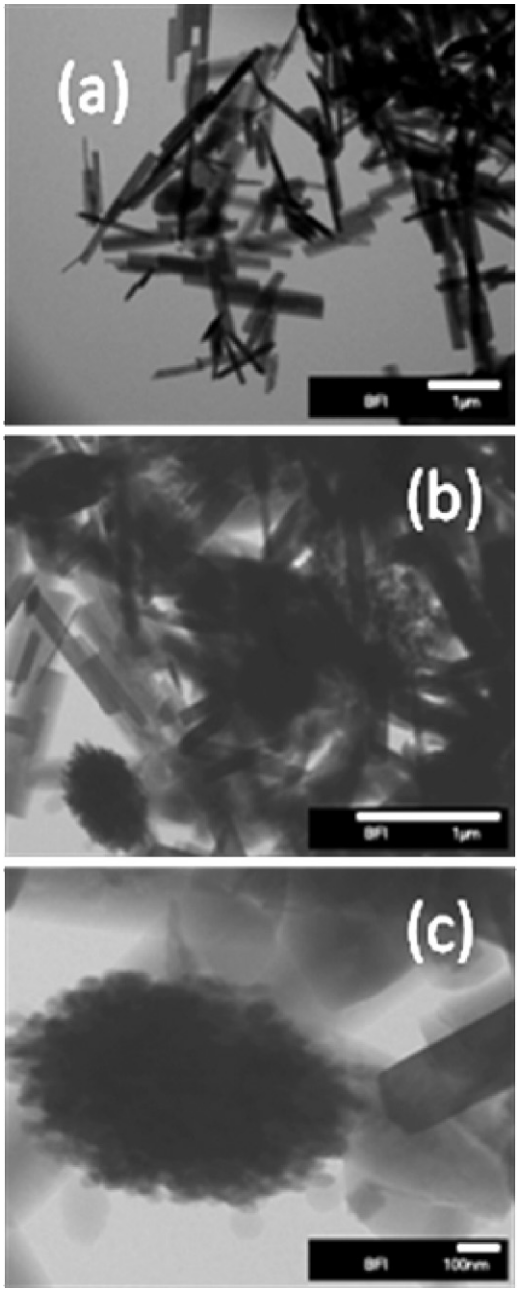

Fig. 1. TEM images of: (a) rod-like Ga/Mg product; (b) Ga/Mg rod-like product mixed with sphere/ellipsoidal aggregates of La/Sr product; (c) detail showing one La/Sr agglomerate formed from nano spherical/ellipsoidal (20–50 nm) particles.

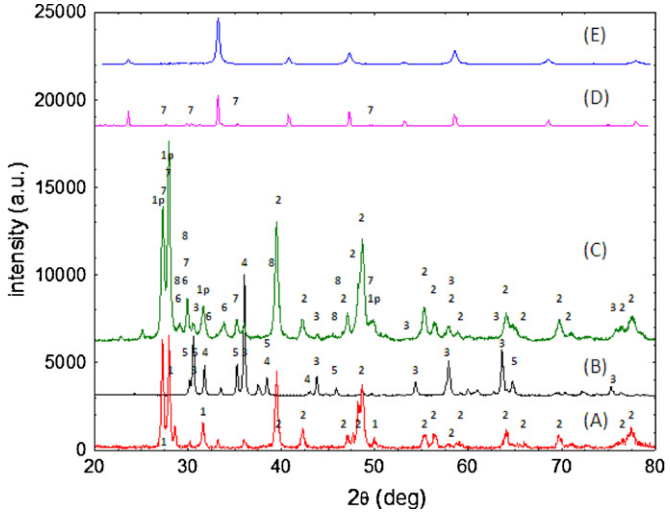

Fig. 2. XRD patterns of (A) La/Sr-product calcinated at 900 °C, (B) Ga/Mg-product calcinated at 900 °C, (C) mixture of La/Sr and Ga/Mg products calcinated at 900 °C, (D) LSGM produced by SPS (37–93 nm), and (E) LSGM commercial pure powder. Phase notation is: 1 = La_2SrO_x [17], 1p = $La_2(Sr, Mg)O_x$ [17], 2 = La-rich oxide phase, 3 = $MgGa_2O_4$ [PDF 10-0113], 4 = Ga_2O_3 [06-0529], 5 = Ga_2O_3 [41-1103], 6 = $Sr_3Ga_4O_9$ [31-1358] or Ref. [17], 7 = $SrLaGa_3O_7$ [45-0637], 8 = La_4SrO_7 [22-1430].

details. Apart from this, heating/sintering regime should be appropriate and designed keeping in mind the specifics of the mixture and processing approach.

Following this idea, the mixture of the La/Sr- and Ga/Mg-based products was conventionally heated up to different temperatures by placing the product into a hot furnace (heating rate was about 150–200 °C/min). In Fig. 2 are presented XRD patterns for the separated and mixed products heat treated at 900 °C.

Phase La_2SrO_x [17] was identified in the La/Sr-product calcinated at 900 °C (pattern A, Fig. 2). This phase is often denoted in literature as unknown and is present in the XRD patterns from different LSGM powders calcinated at 900–1000 °C [18–21]. A La-rich oxide phase (with diffraction peaks at 2θ = 39.51, 47.07, 48.21, 48.64, 55.3, 56.39, 57.87, 58.92, 64.1, 66.05, 69.67, 76.47 and 77.5°), should occur to keep the compositional balance of the La/Sr product, but we could not identify it.

In the Ga/Mg-product calcinated at 900 °C (pattern B, Fig. 2) phases were $MgGa_2O_4$ [10-0113] and various types of Ga_2O_3 (more probable are [06-0529] and [41-1103], but also [43-1013] and [43-1012] are possible).In the XRD pattern taken on the mixed products (pattern C, Fig. 2) identified phases were: La_2SrO_x, La-rich oxide phase, and $MgGa_2O_4$. Probable are also complex oxides $Sr_3Ga_4O_9$ [31-1358, Ref. [17]], $SrLaGa_3O_7$ [45-0637], 8-La_4SrO_7 [22-1430]. Complex oxides have shown shift in the position, change in the intensity and even in the occurrence of the peaks vs. PDF data. This suggests structural and compositional deviations. The amount of phase $MgGa_2O_4$ is low, while Ga_2O_3 was not found. Therefore, these phases are consumed during the calcination process of the La/Sr and Ga/Mg mixture and participate in the formation of complex oxides. In addition, in Ref. [17] peaks belonging to La_2SrO_x and La_2MgO_x have the same 2θ positions and it is thought that a phase 1p = $La_2(Sr, Mg)O_x$ with Mg coming from $MgGa_2O_4$ may form, replacing phase La_2SrO_x [17]. This is also reasonable from the compositional balance considerations. Worthy to note is that identification of the phases is difficult also due to lines overlapping. In the XRD pattern are also present extra peaks, and, hence, formation of intermediate, unknown or metastable phases is possible. LSGM was detected in our mixture after heating at temperatures above 1050–1100 °C.

Based on these results, we designed the SPS thermal regime presented in Section 2, and we established the heating rate from

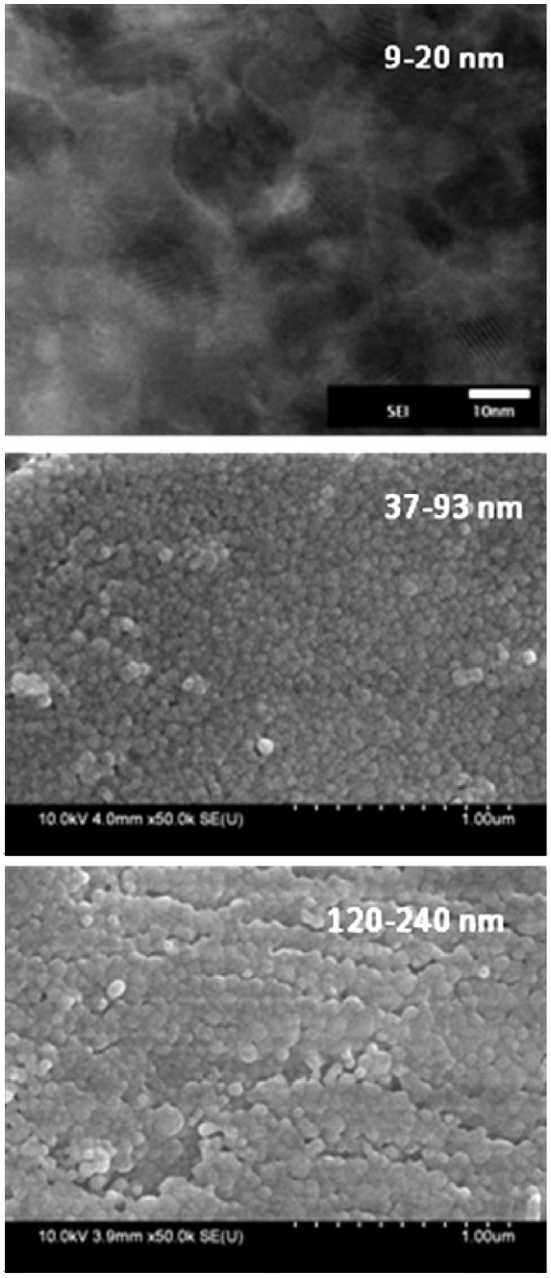

Fig. 3. Low pressure SPS samples of LSGM: TEM (top image) and SEM images of nano sized ceramics.

900 to the final temperature in the SPS processing between 80 and 200 °C/min. It is remarkable that the resulting ceramic is of high density (>90% of the theoretical density), is nano sized (Fig. 3), and it is composed mainly of phase LSGM [24-1102] (Fig. 2, pattern D). However, some impurities can be observed (e.g. $SrLaGa_3O_7$ [45-0637]).

Grains morphology in our SPS ceramic is of equiaxed shape (Fig. 3) with relatively narrow distribution which is likely decreasing for lower particle size: samples heated with rates of 200, 150 and 80 °C/min have shown particle size in the range of 9–20 (average particle size 13 nm), 37–93 (60 nm) and 120–240 nm (140 nm), respectively. For the samples with a larger particle size, SEM reveals round shape edges of the LSGM grains. One significant difference with the microstructure SEM results obtained on high-pressure SPS nano structured samples [10] is that in our case the grain boundaries and the edges of each particle are well-defined. SEM

image from Ref. [10] also shows some well-defined particles, but it mainly reveals sintered blocks of hundreds of nm (≈200 nm) in size. This observation is likely very important for approaching the *conductivity – particle size dependence*, as it will be addressed below. Discrepancy in estimation of the particle size from structural and microscopy data in the nano structured materials were discussed in literature [22,23]. Probably owing to significantly higher applied pressure (700 MPa) and a different reacted precursor (synthesized by Pechini method), in the article [10] authors obtained a higher density (>95%), and LSGM phase formed at lower SPS temperatures (850 °C) than for our case. For our samples, a higher maximum SPS processing temperature (e.g. 1300 or 1350 °C) produced micrometric large particles with well-known polyhedral morphology.

For samples produced at 1200 °C, round-shape edges of the resulting LSGM sphere particles, coarsening of the LSGM particles through a process resembling Oswald ripening, relatively high density achieved within short time and at intermediate sintering temperatures, fast and quite effective conversion into LSGM oxide phase may suggest that during proposed reactive SPS, processes are accompanied by flux or liquid phase processes, at least on the initial stages of the reaction. In addition, low level of mixing between La/Sr and Ga/Mg products was somehow not a critical problem within our proposed route and this is indirectly supporting the same idea of a convenient process associated with the possible presence of a flux/liquid phase. Phase equilibrium diagrams in the LSGM system indicate on the presence of liquid or metastable phases at temperatures close to those used in this work. The binary systems, Ga_2O_3–La_2O_3 and SrO–Ga_2O_3 have eutectics at temperatures as low as 1345 and 1250 °C, respectively ([24] and therein references). Phase $Sr_3Ga_2O_6$ decomposes at 1230 °C [24] (or below 1200 °C according to [37]), and $Sr_3Ga_4O_9$ incongruently melts at 1250 °C [24]. Other phases were reported to melt incongruently at temperatures of 1400–1500 °C [24]. Melting at 1400 °C was observed for samples in the ternary La_2O_3–Ga_2O_3–SrO system [25]. Cong et al. [18] mention without any details a glass phase at grain boundary in LSGM ($La_{0.8}Sr_{0.2}Ga_{0.85}Mg_{0.15}O_x$) synthesized by glycine–nitrate combustion method. For LSGM ($La_{0.8}Sr_{0.2}Ga_{0.9}Mg_{0.1}O_x$) ceramic obtained by high-pressure SPS [10], an amorphous phase is detected from XRD measurements. Sometimes, the phase diagrams are not in perfect agreement with each other. Missing or unsolved details as well as our data are not enough to identify a responsible phase or process as proposed above. Situation is also complicated because, in our case, processing is far from equilibrium. In a first approximation, in our reactive SPS processing approach we take advantage of high heating rates to bring the system in the stability domain of LSGM phase and, thus, to suppress formation of undesired stable impurity phases and evaporation of Ga or Mg. On the other hand, fast heating rates can promote formation of metastable phases that can play the role of flux/liquid phase as suggested above. Low pressure applied during SPS processing helps to squeeze out through evaporation removable volatile components (organic materials and Cl_2), consolidate powder mixture and ultimately to improve the reactive sintering through improving or maintaining the contact between the phases and the particles. While high heating rates and the interplay with pressure may bring non-equilibrium processes into the system, and support and partially explain the proposed scenario, this might not be the full image. It is often noted in the literature that due to pulsed high current used in the SPS technique, unconventional processes are likely to take place strongly influencing interparticle/grain boundary processes [26–30]. Reports are talking about effects of enhanced electro difussion leading to anomalous surface diffusion and to an effect of interparticle/boundary 'cleaning', formation of 'hot' spots promoting nucleation and local gradients for rapid growth, and existence of controversial plasma states and discharges. At current level it is not possible to present a detailed and coherent understanding and more research is required. Nevertheless, due to the specifics of the SPS processing strongly influencing interparticle/boundary regions, it is of much interest to consider application of this technique to LSGM and other nano sized SOFC electrolyte materials.

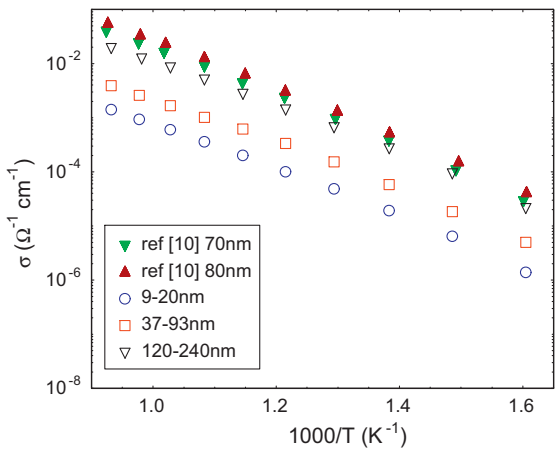

Fig. 4. Total conductivity vs. inversed temperature in (log scale) of our samples produced by reactive SPS with different grain size (estimated by microscopy). Data for high-pressure SPS samples prepared at 850 °C and 900 °C with crystallite size of 70 and 80 nm, respectively, as determined from XRD and reported in Ref. [10] are also shown.

Total conductivity curves vs. temperature in Arrhenius plot representation of our SPS processed LSGM samples with different particle size are presented in Fig. 4. First we shall note that usually presented observations in the literature such as the existence of semicircles in the impedance plots and their behavior with temperature ([10,12] for SPS processed samples) also apply for our samples. A change in the Arrhenius curves slope is observable around 450–650 °C and similar data for SPS samples, 462 °C and 600 °C, were reported in Ref. [12] and [10], respectively. The values of the total conductivity are very similar to those for grain boundary and are lower than the bulk conductivity due to large grain boundary contribution in a fine ceramic. This is as introduced in Refs. [10,12] and due to this we shall not present them in detail.

In the next, we shall focus on the conductivity-particle size relationship. Our data suggest that a higher nano particle size increases conductivity. This tendency is similar to the one presented in Ref. [10]. For convenience, we included in Fig. 4 the data from Ref. [10] obtained for high-pressure SPS processed samples. Revealed tendency is opposite to anticipated nano effects leading to enhanced conductivity especially through the grain boundaries. Before going for more discussions we address the following aspect: apparently there is a large discrepancy between the conductivity values obtained by us and by the authors of Ref. [10]. Our conductivity curve for sample with larger particle size of 120–240 (average 140) nm is quite close to values for samples from Ref. [10] with 'particle size' of 70 and 80 nm (Fig. 4). In fact, in Ref. [10], 70 and 80 nm are the crystallite sizes determined from XRD measurements, and, as already described in the above paragraphs, the average particle size by SEM in these samples is around 150–210 nm, i.e. similar or slightly higher to our 120–240 nm sample. In this circumstance, it is no surprise that data match quite well each other. Apart from the slightly different particle size, the remaining difference, can be attributed to differences inherent to conductivity measurement techniques as noted in Ref. [31] and to different processing conditions leading in the samples to e.g. different density (higher in Ref. [10]), amount of residual phases (lower in Ref. [10]), and others. On the other hand, our conductivity data for the 37–93 nm sample are similar to those reported for the high-pressure SPS sample with particle size of 80 nm from Ref. [12]. Unfortunately, in

the article [12], no details are given on how the particle size was determined and a microscopy image is not available. Presented discussion makes a strong case for necessity to carefully define an electrolyte nano ceramic in order to analyze *the conductivity – particle size dependence*. In most cases, in the literature, particle size is appreciated from SEM data. Even if one applies this criterion, a comparative analysis of the samples produced by different technologies might be misleading because deviations may occur pending on specifics of the materials and used technology.

If the last and important observation is neglected, Omata et al in Ref. [16] show an Arrhenius conductivity graph for YSZ electrolyte in which nano sized samples down to 15 nm particle size and produced by different thin film growth technologies are gathered. A smaller nano size in YSZ produces a higher conductivity, but authors note that this is in contradiction with *space-charge-theory* [32] that would explain enhancement of conductivity for YSZ particle sizes much lower, i.e. less than 1 nm. Another noted problem [16] was that in YSZ, conductivity in sintered samples with particle size of about 20 nm is much lower than in the nano sized thin films of about the same particle size. It is very possible that the boundaries obtained in the material by different synthesis/processing methods behaves in a different way, and for the thin films the influence of the substrate should not be neglected. At the same time, for electrolyte ceria-based HP–SPS ceramic samples with particle size as small as 16 nm, the disappearance of the grain-boundary blocking effect is likely possible [33]. In the ceria-based electrolyte other nano effects are reviewed in Ref. [16].

To have a look on nano effects in LSGM and to make a comparative analysis between nano films and nano sintered bulks is currently not possible. Partly, this is because the films or coatings of LSGM prepared by different methods and reported in the literature [34–38] have a particle size significantly higher than the 100 nm range. To take advantage of nano effects in LSGM, it is possible that particle size should be lower than the minimum particle size obtained in this work of 9–20 nm, or certain boundaries suitable for such effects were not obtained. If one combines our data with literature [19,39–41] ones for $La_{0.9}Sr_{0.1}Ga_{0.8}Mg_{0.2}O_{3-x}$ sintered ceramic with micrometric particle size up to 10 μm and produced by different methods and from different precursors, it can be stated that a larger SEM particle size is improving conductivity. This is due to the decreasing the number of grain boundaries. A similar behavior was observed for a micrometric ceramic [31] with a slightly different composition, $La_{0.9}Sr_{0.1}Ga_{0.9}Mg_{0.1}O_{2.9}$. On the other hand, conductivity was higher in a film with a particle size of 3 μm than for a bulk sample of the same composition with a larger particle size [37]. The film was deposited on $La_{0.8}Sr_{0.2}MnO_3$ (LSM) and a higher conductivity was explained mainly by Mn diffusion from LSM to LSGM film rather than to the difference in the particle size between the film and the bulk.

Systematic experiments to establish the particle *size–conductivity* dependence in LSGM are necessary.

4. Conclusion

We have prepared nano sized $La_{0.9}Sr_{0.1}Ga_{0.8}Mg_{0.2}O_{3-x}$ ceramic with the density higher than 90% through low pressure reactive SPS applied to a mixture of intermediate powdered La/Sr- and Ga/Mg-based products. Products were obtained separately by precipitation and hydrothermal methods, and have shown a sphere- and rod-like morphology, respectively. Despite poor mixing of such powders due to their very different morphology, reactive SPS produced LSGM phase within a short time and with particle size as low as 9–20 nm. Particle size can be controlled through the heating rate and the maximum temperature in the SPS processing. Some ideas are discussed to explain particle, phase and density evolution based on the speculation of a flux or liquid phase occurrence and based on unconventional, non-equilibrium specifics of SPS processing.

Conductivity of our samples was measured, and it was found that a lower particle size in the nano ceramic decreases conductivity level. Considering also literature data this trend is likely valid for particle sizes from 10 μm (or more) down to 10 nm, but a final conclusion cannot be presented. A distinction between microscopy particle size and crystallite grain size should be done when establishing the relationship of conductivity vs. particle size.

A general conclusion is that electrolyte materials require complex and careful optimization pending on specifics of each technology and material(s) and unconventional non-equilibrium methods such as SPS can be very useful. SPS may provide more flexibility in consolidating powders with different initial morphologies and mixing levels than conventional sintering.

Acknowledgements

PB acknowledges support from MANA, Japan and Idei Complexe (9/2010), Romania.

References

[1] T. Ishihara, H. Matsuda, Y. Yakita, J. Am. Chem. Soc. 116 (1994) 3801.
[2] P. Huang, A. Petric, J. Electrochem. Soc. 143 (1996) 1644.
[3] M. Shi, N. Liu, Y. Xu, Y. Yuan, P. Majewski, F. Aldinger, J. Alloys Compd. 425 (2006) 348–352.
[4] R. Polini, A. Pamio, E. Traversa, J. Eur. Ceram. Soc. 24 (2004) 1365.
[5] R. Subastri, T. Mathews, O.M. Sreedharan, Mater. Lett. 57 (2003) 1792.
[6] C. Cristiani, L. Zampori, S. Latorrata, R. Pelosato, G. Donatelli, R. Ruffo, Mater. Lett. 63 (2009) 1892.
[7] B. Rambabu, S. Ghosh, W. Zhao, H. Jena, J. Power Sources 159 (2006) 21.
[8] S.V. Kesapragada, S.B. Bhaduri, S. Bhaduri, P. Singh, J. Power Sources 124 (2003) 499.
[9] M. Ohnuki, K. Fujimoto, Solid State Ionics 177 (2006) 1729.
[10] F. Maglia, U. Anselmi-Tamburini, G. Chiodelli, H.E. Camurlu, M. Dapiaggi, Z.A. Munir, Solid State Ionics 180 (2009) 36–40.
[11] B.W. Liu, Y. Zhang, J. Alloys Compd. 458 (2008) 383.
[12] H.J. Park, C. Kwan, S.M. Lee, Electrochem. Commun. 11 (2009) 962.
[13] P. Majewski, T. Maldener, Int. J. Appl. Ceram. Technol. 6 (2009) 249.
[14] M. Stanislowski, U. Seeling, D.-H. Peck, S.-K. Woo, L. Singheiser, L. Hilpert, Solid State Ionics 176 (2005) 2523.
[15] A. Weber, E. Ivers-Tiffee, J. Power Sources 127 (2004) 273.
[16] T. Omata, Y. Goto, S. Otsuka-Yao-Matsuo, Sci. Technol. Adv. Mater. 8 (2007) 524.
[17] Z.-C. Li, H. Zhong, B. Bergman, Z. Zou, J. Eur. Ceram. Soc. 26 (2006) 2357.
[18] L. Cong, T. He, Y. Ji, P. Guan, Y. Huang, W. Su, J. Alloys Compd. 348 (2003) 325.
[19] H. Ishikawa, M. Enoki, T. Oshihara, T. Akiyama, J. Alloys Compd. 430 (2007) 246.
[20] N. Liu, Y. Yuan, P. Majewski, F. Aldinger, Mater. Res. Bull. 41 (2006) 461.
[21] M. Shi, N. Liu, Y. Xu, Y. Yuan, P. Majewski, F. Aldinger, J. Alloys Compd. 425 (2006) 348.
[22] G.W. Nieman, J.R. Weertman, R.W. Siegel, Nanostruct. Mater. 1 (1992) 185.
[23] J.R. Groza, Nanocrystalline powder consolidation methods, in: C.C. Koch (Ed.), Nanostructured Materials Processing, Properties and Applications, second ed., William Andrew Inc., 2007, pp. 173–229 (Chapter 5).
[24] F. Zheng, R.K. Bordia, L.R. Pederson, Mater. Res. Bull. 39 (2004) 141.
[25] A. Matraszek, L. Singheiser, D. Kobertz, K. Hilpert, M. Miller, O. Schultz, M. Martin, Solid State Ionics 166 (2004) 343.
[26] O. Vasylkiv, H. Borodianska, Y. Sakka, J. Eur. Ceram. Soc. 28 (2008) 927.
[27] S.H. Risbud, J.R. Groza, M.J. Kim, Phil. Mag. B 69 (1994) 525.
[28] J.R. Groza, A. Zavaliangos, Mater. Sci. Eng. A 287 (2000) 171.
[29] J.R. Groza, M. Garcia, J.A. Schneider, J. Mater. Res. 16 (2001) 286.
[30] Grasso, Y. Sakka, G. Maizza, Sci. Technol. Adv. Mater. 10 (2009) 053001.
[31] C. Haavik, E.M. Ottesen, K. Nomura, J.A. Kilner, T. Norby, Solid State Ionics 174 (2004) 233.
[32] X. Guo, R. Waser, Prog. Mater. Sci. 51 (2006) 151.
[33] U. Anselmi-Tamburini, F. Maglia, G. Chiodelli, A. Tacca, G. Spinolo, P. Riello, S. Bucella, Z.A. Munir, Adv. Funct. Mater. 16 (2006) 2363.
[34] Y. Yoo, J. Power Sources 160 (2006) 202.
[35] T.M. He, Q. He, L. Pei, Y. Ji, J. Liu, J. Am. Ceram. Soc. 89 (2006) 2664.
[36] J.W. Yan, M. Enoki, H. Matsumoto, T. Ishihara, Electrochemistry 73 (2005) 945.
[37] R. Pelosato, I.N. Sora, V. Ferrari, C.M. Mari, Solid State Ionics 175 (2004) 87.
[38] K. Sasaki, M. Muranaka, A. Suzuki, T. Terai, Solid State Ionics 179 (2008) 1268.
[39] D. Lee, J.H. Han, Y. Chun, R.H. Song, D.R. Shin, J. Power Sources 166 (2007) 35.
[40] V.V. Kharton, A.L. Shaula, N.P. Vyshatko, F.M.B. Marques, Electrochim. Acta 48 (2003) 1817.
[41] F. Chen, M. Liu, J. Solid State Electrochem. 3 (1998) 7.